Passive Control of Aerodynamic Load in Wind Turbine Blades

Edgar Sousa Carrolo
edgar.carrolo@outlook.com

Instituto Superior Técnico, Lisboa, Portugal

June 2015

Abstract

Large wind turbine blades have many advantages in terms of power efficiency, despite representing an hazard concerning the high loads applied on the structure. Traditionally, there are active control systems that allow blades to adapt according to wind conditions, and so maintain power efficiency and aerodynamic load within acceptable levels. Since the end of the last century, some researchers have been discussing about passive control techniques. The implementation of this kind of aeroelastic response does not bring additional maintenance or weight, unlike active control, because there are no additional devices or complementary structures, and is very useful either to reduce fatigue loads or optimize energy output. The main purpose was to achieve an effective reduction in aerodynamic loading in a wind turbine blade applying the bend-twist coupling concept. In the scope of this work, computational models were developed that simulated the fluid-structure interaction on a enhanced blade model. Coupled analysis considering first only the aerodynamic load and then combining it with inertial were performed. The results demonstrated that this design can reduce aerodynamic load and maximum tip deflection in high wind speeds, thus proving to be a realistic passive control technique.
Keywords: Aerolastic Tailoring, Bend-twist Coupling, Passive Control, Aerodynamic Load, Fluid-structure Interaction

1. Introduction

Until the last quarter of twentieth century, there was in general, little interest to yield electrical energy from wind. In Europe, there were some scarce applications, but the lack of government policies and funds did not contribute to a convergent progress, despite the available technological means.

Since then, several factors contributed to a different view about the use of wind energy. The dramatic rise of oil price forced all entities to seek for alternatives. The wind energy seemed to be a logical investment, since it was used in the past in farms (windmills were used to transform wind energy into mechanical energy) and is available anywhere on Earth. These factors associated with adequate government policies contributed to proliferate these devices to all Europe and North America.

With design focused on turbine mass and cost, it is important to include passive and active techniques to load control, thereby achieve an overall benefit to the system by improving the turbines performance and mitigate both stress and load on the structure.

1.1. Passive Load Control

Whenever a turbine blade is subjected to adverse atmospheric conditions, where extreme wind speeds might occur, the designed load can be far exceeded. This assumption is reinforced when one is dealing with large blades. Therefore, arises the concern in mitigate these loads in order to preserve the structure integrity. In this context, through aerodynamic load control is possible to manage the amount of load carried by the structure, reduce the fatigue damage and thereby enhance the overall efficiency [1]. The bottom idea is change the aerodynamic features of the blade according the atmospheric conditions, namely wind speed.

Passive approach is privileged in sacrifice of active control, since it provides an effective blade unloading without any additional moving parts, in contrast with what happens in active control. The obvious conclusion is that is possible to achieve significant savings in weight. Additionally, all active control systems require further attention in maintenance, because they are rather susceptible to fail than a passive controlled blade design [2]. Thus, these two factors give a definitive contribution to a lower energy cost, associated with significant saving in manufacturing process [3].

1.2. Aerolastic Tailoring

For a long time, wind turbine blades have been built with composite materials, which brings a new set of opportunities regarding the anisotropic properties

of those materials. However, the research in this field is not sufficiently developed, because simulation tools still need improvements to provide more accurate solutions [4].

Goeij [2] in his work gave an elegant definition of aeroelastic tailoring: "the incorporation of directional stiffness into a structural design to control aerolastic deformation, whether static or dynamic, in such a fashion as to affect the aerodynamic and structural performances of that structure in a beneficial way". This design is quite interesting, since it may provide lower fatigue loads with changes in angle of attack with sudden wind gusts. Moreover, the angle of attack may be adjusted to each wind speed and obtain an optimal torque.

1.3. Bend-Twist Coupling

Goeij [2] and his colleagues in the end of last century studied for two different blade configurations. The initial assumptions behind their work is that the blade deforms as reaction to the wind incidence, so it both bends (pure bending) and twist around the rotor's axis. It can twist either in direction to stall, which means that exists an increase in the angle of attack or in direction to feather, that represents a decrease in the angle of attack.

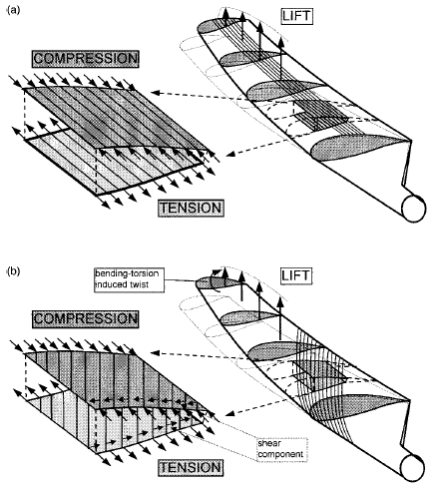

Figure 1: Comparison of a) conventional blade; b) bending-twist coupled blade [2].

A double spar box beam design was presented in their work and it was concluded that the induced twist of this configuration is necessarily lower than a conventional design (single spar), although the objective of maximum load reduction may still be valid. They also stated that bend-twist coupling can be obtained with a base design that includes sweep along the blade. This design creates a moment that induces twist on the blade. Another possible solution is to deviate the composite fibres out of principal axis, sufficiently to generate twist motion and decrease the load applied, taking advantage from the non-isotropic properties of composite materials. The physic mechanism is shown in figure 1

A very recent study [5], working under the latter assumption, investigated the implementation of unbalanced symmetrical stacks of composite layers. The results obtained showed that unbalanced stacks cause higher levels of BTC. The BTC can be quantified from the simplified reduced cross section stiffness matrix:

$$\begin{bmatrix} EI & -S \\ -S & GJ \end{bmatrix} \begin{bmatrix} k_b \\ k_t \end{bmatrix} = \begin{bmatrix} M_b \\ M_t \end{bmatrix}, \tag{1}$$

ere EI and GJ are bending and torsional stiffness, respectively, k_b is the bending curvature, k_t is the rate of twist, M_b and M_t are bending and torsional moment, respectively. S is the coupling stiffness. The normalized BTC coefficient β can be estimated by [5]

$$\beta = \frac{-S}{\sqrt{EI \cdot GJ}} \quad 0 < \beta < 1. \tag{2}$$

In Ashvill's report [6] it is affirmed that bend-twist coupling can reduce fatigue life and limit operating loads. He also concludes that the potential improvement is quite attractive, namely on the structural properties that can be obtained. Nevertheless, further technological improvements, such as CFD and 3D validation tools should be developed, to worth this design manufacturing.

The comparison between stalled and feathered regulated wind turbine blades with bend-torsion coupling were also investigated [7].

2. Aerodynamic Model

2.1. BEM Iterative Solution

As any iterative solution, it is necessary to guess some initial values. In this case, both axial and angular induction factor, a and a' respectively, are be set to zero.

From a velocity triangle, it can be shown [8] that the relative angle ϕ, depends of axial and angular induction factors, a and a' respectively:

$$tan\phi_k = \frac{U(1-a_k)}{\Omega r(1+a'_k)} = \frac{1-a_k}{(1+a'_k)\lambda_r} \tag{3}$$

where k is kth iteration, λ_r is the local tip speed ratio, U is the free-stream wind speed, and Ω is the rotor rotational speed.

It is usual apply the Prantl's tip correction factor in order to account the pressure loss on that region [9], yielding

$$F_k = \left(\frac{2}{\pi}\right) cos^{-1}\left[exp\left(-\frac{(1/2)[1-(r/R)]}{(r/R)sin\phi_k}\right)\right], \tag{4}$$

where R it the rotor radius.

The local angle of attack is computed as

$$\alpha_k = \phi_k - \theta_{T_k} \tag{5}$$

where θ_{T_k} is the total blade pitch angle.

From airfoil data, is possible to extract an interpolated C_l value and conclude the iterative process updating new values a and a', closing the loop with the following expressions:

$$a_{k+1} = \frac{1}{1 + \frac{4F_k sin^2(\phi_k)}{\sigma C l_k cos\phi_k}}, \quad a'_{k+1} = \frac{1}{\frac{4F_k cos(\phi_k)}{\sigma C l_k} - 1} \tag{6}$$

This set of routines should be executed until convergence criterion is reached.

2.2. Numerical Model

During the course of this work, it became important automate the aerodynamic force computation regarding a fixed wind speed. Therefore a numerical tool in the commercial tool $MATLAB^{®}$ was developed, to obtain a pressure distribution in a blade surface, following the principles of panel method and BEM.

2.3. Pressure distribution

From the input variables, the algorithm developed runs on background an auxiliary software *XFoil*. This tool applies a 2-D panel method, in inviscid and incompressible flow conditions. The software receives input flow conditions, such as free-stream wind speed, air density, Reynolds number and Mach Number. Additionally, the airfoil section coordinates are necessary to perform the aerodynamic analysis. Then, the software does the analysis and save the C_p output files, one per angle of attack. Since the blade operational angle of attack is initially unknown, this range should be sufficiently large to include the converged value obtained by BEM later on.

2.4. BEM Computation

The implementation of BEM is followed step by step as presented in section 2.1. Recalling equation (5), it is important to explain in detail the components of θ_{T_i}. The total blade pitch angle has three origins,

$$\theta_r = \theta_{0_r} + \theta_{a.c._r} + \beta_r \tag{7}$$

whereθ_{0_i} is the designed twist angle and it is a section property (so its value remains constant), $\theta_{a.c._i}$ is the active control pitch angle (it also remains constant during all iterations but should be set in the beginning of the simulation). β_i is the twist of structural reaction. In each solution of BEM, θ_i remains constant, but will vary due to surface deformation, whenever both aerodynamic and structural models are coupled.

The converged value of angle of attack allows the access of C_p database created by *XFoil*, and a pressure distribution to all blade surface.

2.5. Aerodynamic Load Computation

The aerodynamic load is directly obtained from the pressure distribution. The non-dimensional parameter of this quantity in the jth panel is given by

$$C_{p_{r,j}} = \frac{p_{r,j} - p_0}{\frac{1}{2}\rho U^2}, \tag{8}$$

where the p_j is the pressure in the jth panel of a radial position r, p_0 is the atmospheric pressure. The pressure due to the fluid-interaction is given by dropping p_0, thus yielding

$$p_{r,j} = C_{p_{r,j}} \frac{1}{2}\rho U^2. \tag{9}$$

The aerodynamic model general routine is presented in the figure 2.

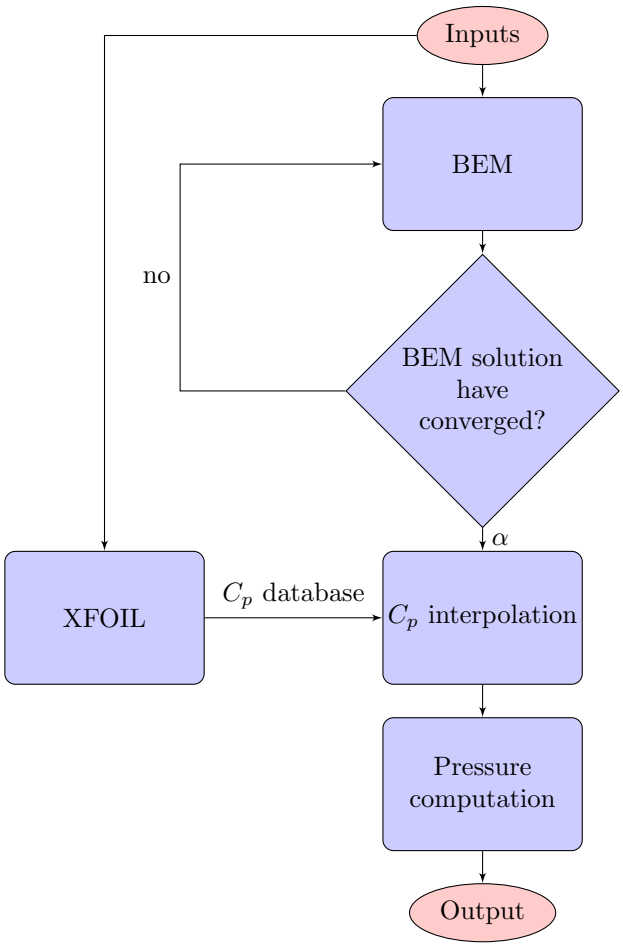

Figure 2: Fluxogram about aerodynamic model framework.

3. Structural Model

The solution of finite elements seek to find the minimum total potencial energy Π:

$$\begin{aligned}\Pi &= \frac{\partial}{\partial q}\left(\int_V \frac{1}{2}\{\varepsilon\}^T\{\sigma\}dv\right)\\ &\quad -\frac{\partial}{\partial q}\left(\int_V \{u\}^T p^V dV\right)\\ &\quad -\frac{\partial}{\partial q}\left(\int_S \{u\}^T\{p^S\}dS\right) \qquad (10)\end{aligned}$$

Computing the strains and stress relations and substituting in the above equation, yields [10]

$$\begin{aligned}\Pi &= \frac{\partial}{\partial q}\left(\int_V \frac{1}{2}\left([B]\{q\}\right)^T[E]\left([B]\{q\}\right)dV\right)\\ &\quad -\frac{\partial}{\partial q}\left(\int_V \left([N]\{q\}^T\right)\{p^V\}dV\right)\\ &\quad -\frac{\partial}{\partial q}\left(\int_S \left([N]\{q\}^T\right)\{p^S\}dS\right). \qquad (11)\end{aligned}$$

The differentiation relative to nodal displacement q, is given by

$$\begin{aligned}&\int_V [B]^T[E][B]dV\{q\}\\ &-\int_V [N]^T\{p^V\}\int_S [N]^T\{p^S\}dS = 0, \qquad (12)\end{aligned}$$

Each integral has a significant meaning:

$$[K] = \int_V [B]^T[E][B]dV\{q\}, \qquad (13)$$

$$\{f\} = \int_S [N]^T\{p^S\}dS, \qquad (14)$$

matrix $[K]$ is called *element stifness matrix*, $\{f\}$ and is the *force vector*.

Usually, for one element is applied the following notation:

$$[k]\{q\} = \{f\}, \qquad (15)$$

Once obtained all element equations, it is necessary to assemble them in one single system of equations to reach the final solution. Therefore, the global system of equations is give by

$$[K^G]\{Q^G\} = \{F^G\}, \qquad (16)$$

and the total minimum potential energy is simply the sum of element potential energies:

$$\Pi^G = \sum_{i=1}^{num.\ elem} \Pi_i \qquad (17)$$

3.1. Numerical Model

The numerical code developed in $MATLAB^{®}$ builds from a set of inputs defined by the user, a structured mesh of a wind turbine blade. An output file with *APDL* code is created and computed in the FEM tool $ANSYS^{®}$, that performs a static simulation and gives the solution regarding the blade structural response.

3.2. Input Variables

The initial inputs necessary to compute the mesh are the number of elements along the blade chord, span and webs. Additionally, user may change the web position (in percentage of chord). Furthermore, all coordinates concerning airfoil sections should be in percentage of chord and located in a *.txt* file.

3.3. Nodes Assembly

The first action taken by $MATLAB^{®}$ is to compute the blade sections. The code reads the airfoils output files and draws them.

The amount of data collected to build the blade geometry assumes a special relevance, namely about the number of airfoil sections collected to build it. The accuracy in the interpolation is improved if more sections are loaded previously, otherwise trailing edge position can suffer significant deviations. Identically, it is also important to have a sufficiently large number of points per file, as it may affect negatively the interpolation of intermediate chord coordinates. Nevertheless, the user has freedom to choose the number of divisions in chord, span and webs, then from the set of computed airfoil sections, all nodes are generated by linear interpolations of two neighbour sections.

3.4. Elements Assembly

Followed by nodes data, $ANSYS^{®}$ needs to know which are the nodes the form each finite element. Therefore, a routine to assemble all the elements was developed. The element chosen was *SHELL181*, that is the one most suitable to shell structures. It is constituted by four nodes, so starting in the leading edge of root section in suction side, a sweep is done towards trailing edge to compute a line of elements.

The direction in which the nodes are computed is not arbitrary, since the unitary normal vector in $ANSYS^{®}$ follows the right hand rule, this way the routine implemented guarantees that it is always pointing toward the positive Y-axis of the local reference frame. That fact is determinant to compute surface loads, once a positive pressure load is applied in the opposite direction of the element unitary normal vector. Furthermore, in case of using composite materials, the stack sequence is oriented according the orientation of this vector. As soon as the sweep towards trailing edge is done, the span

coordinate is incremented and the same routine applied two times the number of span divisions defined by the user (one at suction side, the other at pressure). The total number of elements covering the blade surface is then two times the product between the divisions in chord and span. The same set of routines is applied to compute the webs elements.

4. FSI Model

4.1. Loose Coupling FSI Method

The critical point of fluid structure interaction is the transfer of information between aerodynamic and structural grids, in particular, transfer the aerodynamic load to the structural grid and the displacement field to the aerodynamic grid. The main criterion that should be guaranteed is that both aerodynamic and structural meshes are flawlessly connected, thus:

$$u_{s_k} = u_{a_k}, \tag{18}$$

where u_{s_k} is the position vector of an arbitrary node of the structural grid and u_{s_k} is the similar accounting the aerodynamic grid.

The structural solver should be able to solve the equation of motion,

$$[M]\{\ddot{q}\} + [G]\{\dot{q}\} + [K]\{q\} = \{F\}, \tag{19}$$

where $[M]$, $[G]$ and $[K]$ are the mass, gyroscopic and stiffness matrices. $\{F\}$ is the force vector. Under steady axial flow conditions, the blade has a constant aerodynamic load and the motion equation is resumed to the equation (16). Vector $\{F\}$ contains forces from different natures:

$$\{F\} = \{F_0\} + \{F_g\} + \{F_{aero}\} + \{F_{n.l.}\} \tag{20}$$

where $\{F_0\}$ is the constant force, $\{F_g\}$ is the gravitational load, $\{F_{aero}\}$ and $\{F_{n.l.}\}$ is the non-linear component. Let us assume that the unique constant force is $\{F_{aero}\}$, and neglect $\{F_{n.l.}\}$ and $\{F_g\}$. The static equilibrium is given by

$$[K]\{q\} = \{F_{aero}\}, \tag{21}$$

which has the same meaning of equation (15). $\{F_{aero}\}$ is obtained from the aerodynamic module.

Dong Ok Yu and Oh Joon Kwon [11] presented in their research one simple loose coupling FSI method of simple implementation. Consists on a static FSI model running in sequence both structural and aerodynamic models, the former assisted by a CFD tool. The structural mesh is initially undeformed and CFD tool calculates the aerodynamic load for the undeformed structure. Then, the output of CFD solver is coupled in the FEM tool that will apply the aerodynamic load on the deformed mesh and provide a new output relatively to an updated deformed mesh, which will be returned in CFD solver. The iterative process is repeated until the convergence of $\{F_{aero}\}$ and displacement vector $\{q\}$ have been verified.

Since the objective of this work is observe a mitigation in load due to the BTC, in this model only twist is coupled, whereas in a conventional FSI coupling model, where both displacements and rotations are coupled. Thus, the load mitigation will be achieved exclusively by the variation in twist.

The coupling is initiated by the FE tool. The aerodynamic load is treated in $ANSYS^{®}$ as a pressure load on the elements and both aerodynamic and structural meshes are coincident, as stated by the expession 18. $ANSYS^{®}$ simulation consists in a steady static analysis of the structure and the the nodal displacement field is returned to the $MATLAB^{®}$.

From the nodal displacements, it is possible to infer about the amount of twist that the blade is subjected. A correct twist computation would be calculating it in relation to the elastic axis, however it is not possible to determine precisely where it is located. Therefore this angle was calculated taking into account the displacement of leading and trailing edges in each span coordinate,

$$\beta_i = arctan\left(\frac{y_{i_{t.e.}} - y_{i_{l.e.}}}{x_{i_{t.e.}} - x_{i_{l.e.}}}\right). \tag{22}$$

where $y_{i_{l.e.}}$ is the y position of the leading edge, $y_{i_{t.e.}}$, is the y position of the trailing edge. The same notation is applied to $x_{i_{l.e.}}$ and $x_{i_{t.e.}}$.

β_i is updated in the BEM solver, which initially is set to zero and will make the aerodynamic load change in each iteration. The updated $\{F_{aero}\}$ is then introduced in $MATLAB^{®}$ and the iterative process is consecutively executed until $\{F_{aero}\}$ converge.

The generic coupling sequence is represented in figure 3, and shows the framework of all numerical models developed during the course of this work.

5. Baseline Design

5.1. Wind Turbine NREL 5 MW Data

The blade is constituted by a mixture of TU Delft and NACA airfoil shapes, while the root region contains circular sections. The transition region is not clearly documented. In table 1 it is possible to consult the different airfoils used in the NREL 5MW blade.

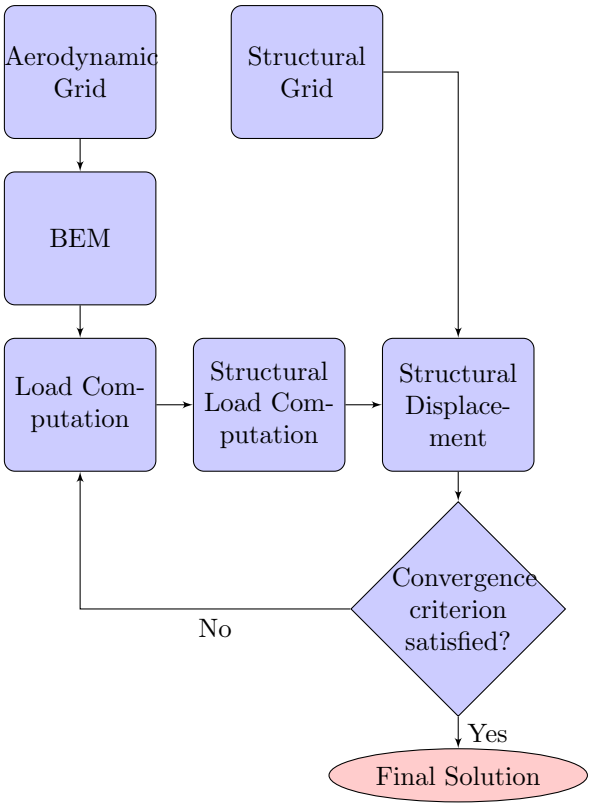

Figure 3: Fluxogram about BEM iterative solution

Airfoil	$[\%t/c]$	z $[m]$)	Airfoil ID
Cylinder 1	100	1.8	1
Cylinder 2	100	5.98	2
DU W-405	40.5	10.15	3
DU 97 W-300	35.09	15.00	4
DU 91 W2-250	30	20.49	5
DU 91-W2-250	25	26.79	6
DU 91 W-210	21	34.22	7
NACA 64-618	18	42.47	8

Table 1: NREL 5MW wind turbine blade airfoils [12].

The mixture of materials commonly known as E-glass/epoxy is quite frequent in wind turbines applications, whose mechanical properties are available in table 2. This material was applied in the FE tool, considering laminates with constant thickness, 8 layers oriented in the blade plane, +45 degrees in relation to the edgewise axis.

The free-stream wind velocity was set to 25 m/s, equal to catalogued rotor cut-out speed, and crosses the blades from the leading to the trailing edge, as usual.

[1]Estimated value

Density ρ [kg/m^3]	1920
Longitudinal Modulus E_{11} $[GPa]$	43.2
Transversal Modulus E_{22} $[GPa]$	12.6
Poisson Coefficient ν	0.38
Distorsion Modulus G $[GPa]$	4.2
Yield strength σ_y $[GPa]$	176.6 [1]

Table 2: E-glass/Epoxy composite elastic properties [5].

5.2. Parametric Study Summary

A parametric study was done, following the implementation presentation previously. The main goal was to build an enhanced blade design that can provide the highest twist, and still maintain an acceptable global structural response. The adopted criteria to compute the enhanced design was whether it was possible exclusively from the results demonstrated from the parametric study.

The parameters under study were:

- **Fibres layers orientation**; varying initially, all fibre layers resulting in an unidirectional laminate. Then it were developed three multi-directional stacks: one balanced and two unbalanced;
- **Thickness distribution**; it was essentially compared the response between a constant distribution and two variable distributions;
- **Number of shear webs and location**; it were distinguished four different cases, where it was varied the number of webs from zero to two, and in the latter two different position were investigated, maintaining the relative distance between them constant;
- **Material reinforcement**; it was implemented besides the e-glass/epoxy composite, a carbon fibre composite, with distinguished elastic properties in two of the most interior layers of the laminate.

All the evaluated parameters proved to be quite relevant to blade structural behaviour. The fibres orientation is one parameter that might be adjusted as function of the stiffness required locally, and can provide significant improvements in the overall performance.

The thickness is probably the most sensitive and unpredictable parameter of all studied, as a refinement in specific zone must be evaluated regarding the all blade performance, avoiding the possibility of comparison of independent regions.

The influence of the number of webs was not completely clarified, but it was made clear the importance of having them in hollows structures. The

structural response by single and double web configurations were very similar, so no obvious can be extracted about which one can provide the best solution according the desired proposal.

The reinforcement done with carbon fibres demonstrated in significant improvements, namely in the induced twist, whereby it is definitely a solution to consider in an enhanced design.

6. Enhanced Design

Following the findings in section 5, the fibres orientation should be in a such way, that can provide both flapwise stiffness and induced twist on the blade. Therefore, assuming that the blade root is subjected to high flapwise moments, it was introduced all layers with 90° fibres, (longitudinal direction), so a high longitudinal stiffness can be achieves with this layup. The root laminate stack is presented in figure 4.

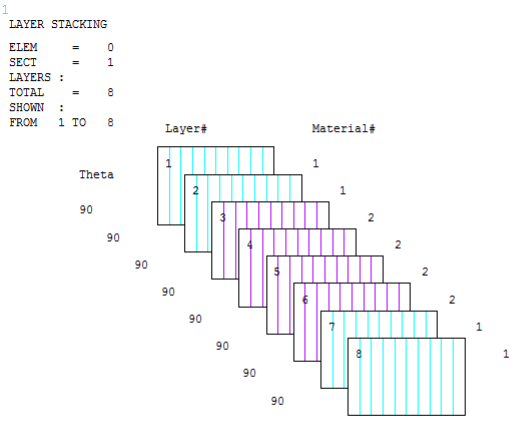

Figure 4: Root laminate stack.

Ideally, the remain blade surface should be covered by layers with -45° fibres, but buckling issues might occur and for that reason, usually real blades have layers with longitudinal fibres [13]. Hence, it was applied a stack to the blade surface as in figure 5. The region right next to the root, between 10 and 20m, has shown to be a region of structural demand, thus two additional longitudinal fibres were employed, replacing -45° fibres, creating an intermediate solution between root and tip stacks, as illustrated in figure 6.

The thickness distributions of figure 7 was previously tested during the parametric study. It caused a great loss of stiffness, but the author believes that the positives effects of the new laminate stack, will mitigate adverse effects of having this thickness distribution.

The shear webs position was changed in relation to the baseline design, although the double web con-

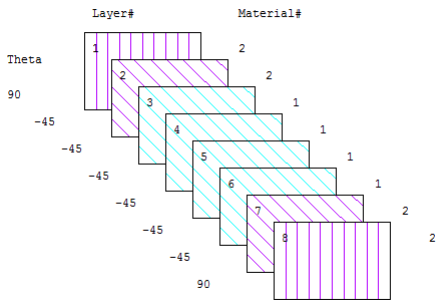

Figure 5: Mid-span laminate stack.

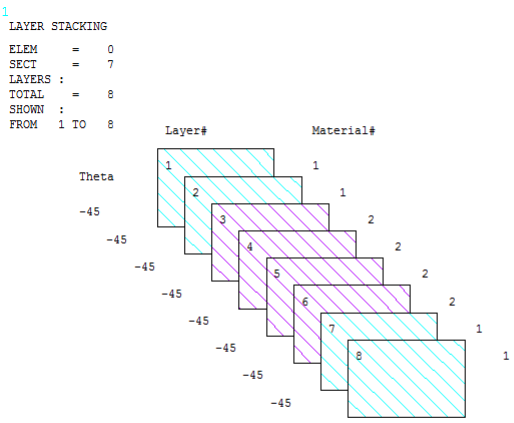

Figure 6: Tip laminate stack.

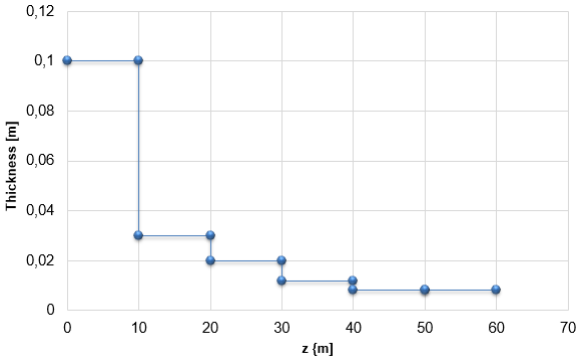

Figure 7: Enhanced blade thickness distribution.

figuration has been maintained. The argument of this modification has to do with the lack of effectiveness demonstrated by the shear web located closer to the trailing edge. Despite, the good performance evidenced by the single shear web configuration, it is not clear that this performance could be consistent when a variable thickness distribution was introduced. Furthermore, in the research that supported this work, the double web configuration is rather used than single one. Further studies would

be necessary to abandon this conservative solution.

Finally, regarding the reinforcement done with the composite of table 3, it revealed to be successful, and it was integrated in the laminates stack, as shown in figures 4 to 6 labelled by material 2. At the root, the interior layers were changed to carbon composite, and the remaining blade span included carbon fibres not only in the longitudinal layers but also in the interior layers containing oblique fibres.

Density ρ $[kg/m^3]$	1590
Longitudinal Modulus E_{11} $[GPa]$	155
Transversal Modulus E_{22} $[GPa]$	9
Poisson Coefficient ν	0.3
Distorsion Modulus G	3.5
Yield strength[2] σ_y $[MPa]$	633.4

Table 3: Carbon(T300)/epoxy composite mechanical properties [5].

7. Coupled Analysis

This analysis consisted on an iterative solution, coupling the $\Delta\beta$ into the aerodynamic model to obtain an updated surface load. The simulation has been ran until converged results have been verified.

7.1. Structural Performance

With five iterations it was possible to get a converged solution, regarding nodal displacements and twist distribution.

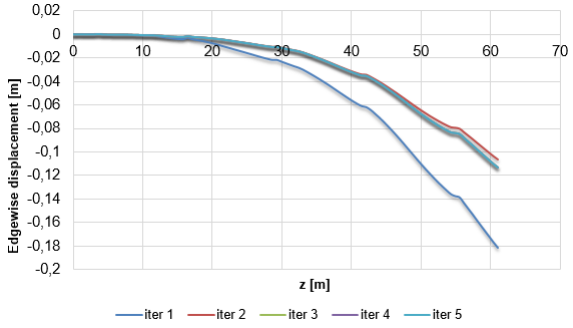

Figure 8: Enhanced blade: edgewise displacement at $(^x/_c) = 25\%$.

The results show that the aerodynamic load can effectively be mitigated with this design, and produce significant reductions in both flapwise and edgwise displacement, which is visible in figures 8 and 9. The twist distribution in figure 10 is also lower when the solution is converged, but that difference is not so noticeable.

The stress distribution, in figure 11 shows that the reinforcement applied after the root region was

[2]Estimates value.

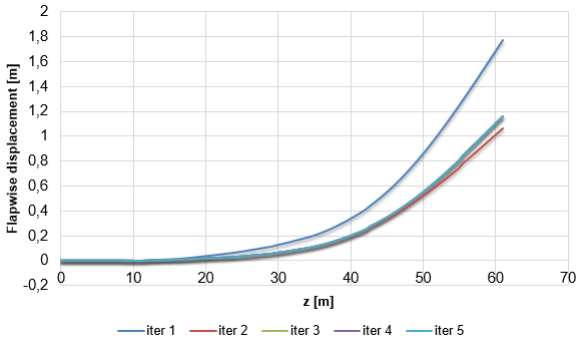

Figure 9: Enhanced blade: flapwise displacment displacement at $(^x/_c) = 25\%$.

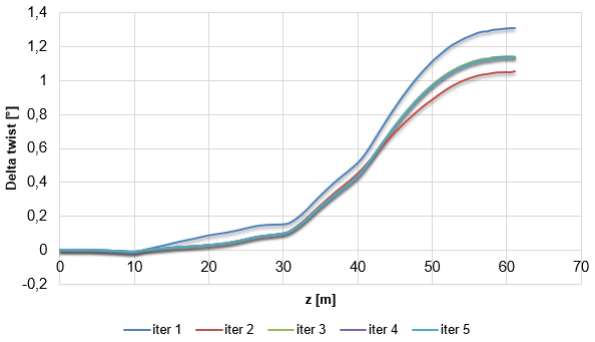

Figure 10: Enhanced blade: twist distribution.

not sufficient to mitigate the high stresses in that region, although the maximum value exhibited in table 4, is clear lower than the estimated yield strength of the composite. Anyway, further investigations should be done in this particular point, as some researchers [2], [1] affirm that designs implemented high levels of BTC can increase fatigue loads. Therefore, the impact of this stress in fatigue lifetime should be evaluated.

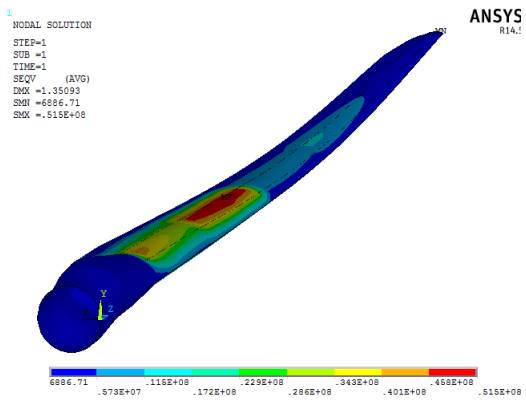

Figure 11: Enhanced blade: von Mises stress plot.

The estimated initial total load in upper and lower blade surfaces were

Iter.	y_{max} $[m]$	x_{max} $[m]$	β_{max} $[^\circ]$	σ_{max} $[M$
1 to 5	2.05	-0.20	1.31	59.2
5	1.35	-0.12	1.14	50.8

Table 4: Enhanced blade: maximum values.

$$|F_{upper}| = 87.3\ kN \quad and \quad |F_{lower}| = 33.5\ kN.$$

In the end of coupled analysis, these values were

$$|F_{upper}| = 85.0\ kN \quad and \quad |F_{lower}| = 33.4\ kN,$$

resulting in total aerodynamic load reduction of 2.1%. This result is explicit about the interest about the mitigation of aerodynamic load since, with small savings, it is possible to achieve less demanding structural requirements.

8. Static Analysis including Inertial Loads

This final analysis aims to give an insight about the impact of inertial loads on the blade response.

This analysis followed exactly the some procedures of previous one, but in this case it was considered an extreme case, where aerodynamic, gravitational and gyroscopic loads are acting in the same direction, with the blade parallel to the ground.

The maximum tip deflection in [13] was 8.46 m, for a rotating situation. In that work, it was being analysed a 70 m blade, also developed by NREL, with identical geometrical features. Thus, it is acceptable to make a linear re-scaling to have a reference value about the maximum tip deflection of the blade one is working. The estimated value was 7.25 m. In [13], it is also applied a safety factor of 1.35 in all forces, but for convenience, in this analysis it was applied the same safety factor to the maximum tip deflection, yielding 5.37 m. The reference angular velocity used during the simulations is the rated rotor speed, 12 rpm.

The same trends verified in the previous analysis are visible in figures 12 to 14. The main differences lie on maximum absolute values, that are quite superior due to the introduction of additional sources of load. The reference maximum tip deflection is not reached, but it should be noted that, other types of load can still be added to the ones considered so far, which may induce even higher displacements.

The increase in total load is also reflected on the stress exerted on the blade. The distribution is similar to the previous analysis, but while in that one the maximum stress clearly below the estimated yield strength, the actual load yields a maximum much closer to this boundary. Furthermore, applying the same safety factor to the composite yield, in

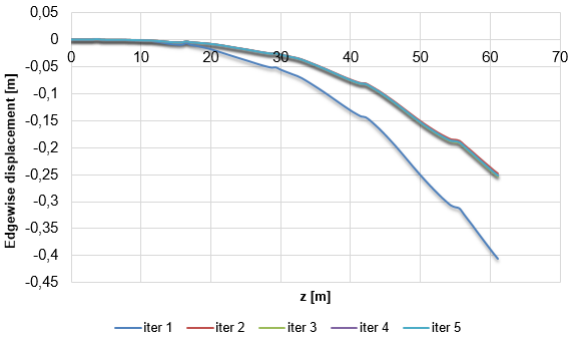

Figure 12: Enhanced blade including inertial loads: flapwise displacement at $(^x/_c) = 25\%$.

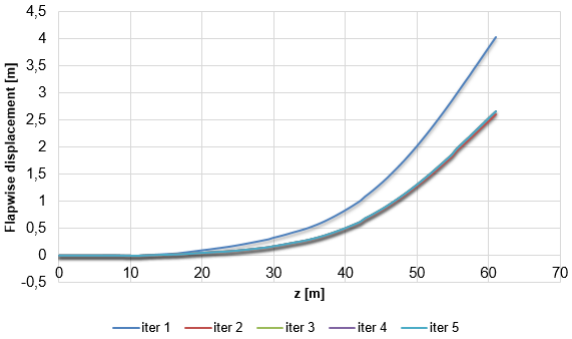

Figure 13: Enhanced blade including inertial loads: edgewise displacement at $(^x/_c) = 25\%$.

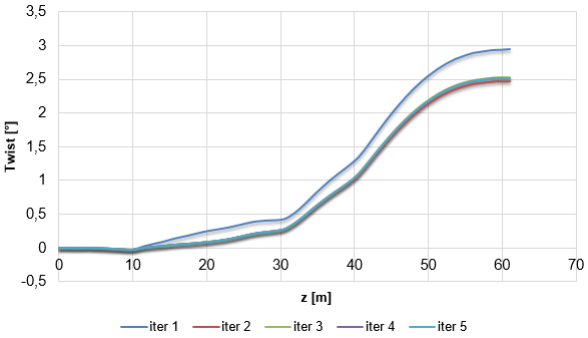

Figure 14: Enhanced blade including inertial loads: twist distribution.

fact this threshold is exceeded. Similarly as what happens in figure 11, from the stress plot of figure 15 is evident an overstressed region next to the root, due not only to the insertion zone of webs, but also where high suction zones are found. Therefore, for a more conservative approach is prudent, to reinforce this zone either by changing some of the oblique layers by longitudinal layers, or alternatively make a slight adjustment in laminate thickness.

9. Conclusions

The design presented in this work focused in a blade configuration the could provide the maximum twist

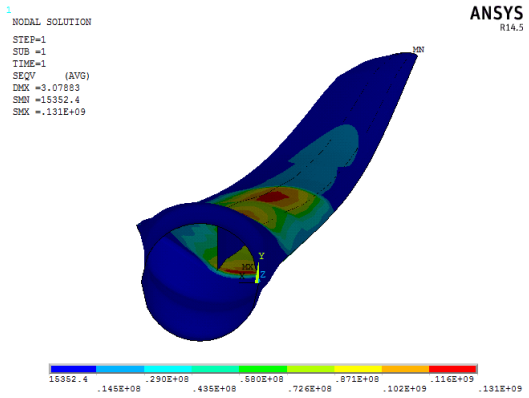

Figure 15: Enhanced blade including inertial loads: von Mises stress.

possible, in a such way that applying the BTC concept could achieve an effective aerodynamic load reduction. This reduction is particularly visible in lower maximum displacements and stresses in the structure.

The developed enhanced design was justified from the conclusions of the parametric study and confirmed its proposals. Besides the reduction of total aerodynamic load through the coupling of induced self twist, both blade flapwise and edgewise maximum deflections were reduced with this design. Taking into account the reference values, and all the developed reasoning, it has been shown that the blade stiffness was correctly dimensioned, as the maximum stress ranged below the material yield strength.

The integration of inertial loads in the analysis has confirmed that these source of loads are quite relevant in design stage, as represent a significant part of total load exerted upon the blade. This design maintained enough sturdiness to keep maximum displacements below reference values, so a sort of static validation of this model was performed successfully.

Acknowledgements

The author would like to thank to professor André Marta for his constant availability and the confidence environment he has created to expose my doubts, problems and concerns. Likewise, a thank should be given to the Ph D. student Simão Rodrigues for his technical help.

References

[1] Don W. Lobitz and Paul S. Veers. Load Mitigation with Bending/Twist-coupled Blades on Rotors using Modern Control Strategies. *Wind Energy*, 6(2):105–117, 2003. doi: 10.1002/we.74.

[2] W.C. de Goeij, M.J.L. van Tooren, and A. Beukers. Implementation of bending-torsion coupling in the design of a wind turbine rotor blade. *Journal of Applied Energy*, 2:191–207, 1999.

[3] E Muljadi, K Pierce, P Migliore, National Wind, and National Renewable. Control strategy for varaible-speed Stall-Regulated Wind Turbines. *NREL Laboratories*, 1998.

[4] Christian Deilmann. Passive aeroelastic tailoring of wind turbine blades - A numerical analysis -. Master's thesis, Massachussets Institute of Technology, 2009.

[5] Manudha T. Herath, Aaron K.L. Lee, and B. Gangadhara Prusty. Design of shape-adaptive wind turbine blades using differential stiffness bend-twist coupling. *Ocean Engineering*, 95:157–165, February 2015. doi: 10.1016/j.oceaneng.2014.12.010.

[6] Tom Ashwill. Passive Load Control for Large Wind Turbines. *51st AIAA/ASME/ASCE/AHS/ASC Structures, Structural Dynamics, and Materials Conference*, pages 1–12, 2010. doi: 10.2514/6.2010-2577.

[7] Andrew T Lee, B E Hons, and Richard G J Flay. Compliant blades for wind turbines. *IPENZ Conference*, 1998.

[8] Martin O. L. Hansen. *Aerodynamics of Wind Turbines*. EARTHSCAN, 2 edition, 2008. 978-1-84407-438-9.

[9] John D. Anderson. *Fundamentals of Aerodynamics*. Mc Graw Hill, 3rd edition, 2001. ISBN 0-07-237335-0.

[10] G. P. Nikishkov. *Introduction To The Finite Element Method*. Lecture Notes UCLA, 12 edition, 2004.

[11] Dong Ok Yu and Oh Joon Kwon. Predicting wind turbine blade loads and aeroelastic response using a coupled CFD-CSD method. 70:184–196, 2014. doi: 10.1016/j.renene.2014.03.033.

[12] Brian R Resor. Definition of a 5MW / 61 . 5m Wind Turbine Blade Reference Model. 2013.

[13] Kevin Cox and Andreas Echtermeyer. Structural design and analysis of a 10MW wind turbine blade. *Energy Procedia*, 24(1876):194–201, 2012. doi: 10.1016/j.egypro.2012.06.101.